CGILS: Results from the First Phase of an International Project to Understand the Physical Mechanisms of Low Cloud Feedbacks in General Circulation Models

Minghua Zhang[1], Christopher S. Bretherton[2], Peter N. Blossey[2], Phillip H. Austin[3], Julio T. Bacmeister[4], Sandrine Bony[5], Florent Brient[5], Suvarchal K. Cheedela[6], Anning Cheng[7], Anthony D. Del Genio[8], Stephan R. De Roode[9], Satoshi Endo[10], Charmaine N. Franklin[11], Jean-Christophe Golaz[12], Cecile Hannay[4], Thijs Heus[6], Francesco Alessandro Isotta[13], Dufresne Jean-Louis[5], In-Sik Kang[14], Hideaki Kawai[15], Martin Koehler[16], Vincent E. Larson[17], Yangang Liu[10], Adrian P. Lock[18], Ulrike Lohman[13], Marat F. Khairoutdinov[1], Andrea M. Molod[19], Roel A.J. Neggers[20], Philip Rasch[21], Irina Sandu[6,16], Ryan Senkbeil[17], A. Pier Siebesma[20], Colombe Siegenthaler-Le Drian[13], Bjorn Stevens[6], Max J. Suarez[19], Kuan-Man Xu[7], Knut von Salzen[22], Mark J. Webb[18], Audrey Wolf[23], Ming Zhao[12]

CORRESPONDING AUTHOR:

Minghua Zhang, Institute for Terrestrial and Planetary Atmospheres, Stony Brook University, Stony Brook, NY 11794-5000. Email: minghua.zhang@stonybrook.edu

[1]Stony Brook University, USA

[2]University of Washington, USA

[3]University of British Columbia, Canada

[4]National Center for Atmospheric Research, USA

[5]Laboratoire de Meteorologie Dynamique/Institute Pierre Simon Laplace (IPSL), France

[6]Max Planck Institute for Meteorology, Hamburg, Germany

[7]NASA Langley Research Center, USA

[8]NASA Goddard Institute for Space Studies, USA

[9]Delft University of Technology, The Netherlands

[10]Brookhaven National Laboratory, USA

[11]Centre for Australian Weather and Climate Research, Commonwealth Scientific and Industrial Research Organisation (CSIRO), Australia

[12]NOAA Geophysical Fluid Dynamics Laboratory, USA

[13]Swiss Federal Institute of Technology, Switzerland

[14]Seoul National University, Korea

[15]Meteorological Research Institute, Japan.

[16]European Centre for Medium-Range Weather Forecasts, United Kindom

[17]University of Wisconsin -- Milwaukee, USA

[18]Met Office Hadley Centre, United Kingdom

[19]NASA Goddard Space Flight Center, USA

[20]Royal Netherlands Meteorological Institute (KNMI), the Netherlands

[21]Pacific Northwest National Laboratory, USA

[22]Canadian Centre for Climate Modelling and Analysis, Canada

[23]Columbia University, USA

ABSTRACT

CGILS – the CFMIP-GASS Intercomparison of Large Eddy Models (LESs) and Single Column Models (SCMs) – is an international project in which most major climate modeling centers participated to investigate the mechanisms of cloud feedback in SCMs and LESs under idealized climate change perturbation. This paper describes the CGILS results from 15 SCMs and eight LES models. Three cloud regimes over the subtropical oceans are studied: shallow cumulus, cumulus under stratocumulus, and well-mixed coastal stratus/stratocumulus. SCMs simulated a wide range of cloud feedbacks in all regimes. In the stratocumulus and coastal stratus regimes, models without activated shallow convection generally simulated negative cloud feedbacks, while models with active shallow convection generally simulated positive cloud feedbacks. In the shallow cumulus regime, this relationship is less clear, likely due to the larger cloud depth and different parameterization of lateral mixing of clouds. The majority of LES models simulated negative cloud feedback in the well-mixed coastal stratus/stratocumulus regime, and positive feedback in the shallow cumulus and stratocumulus regime. A general framework is provided to interpret SCM results: In a warmer climate, the moistening rate of the cloudy layer associated with the surface-based turbulence parameterization is enhanced, which alone causes negative cloud feedback, while the drying rate associated with the shallow convection scheme or cloud-top entrainment parameterization is also enhanced, which alone tends to cause positive cloud feedback. The net cloud feedback depends on how these two opposing effects counteract each other. The CGILS results highlight the need to treat physical parameterizations in General Circulation Models (GCMs) as systems rather than individual components.

1. Introduction

Cloud-climate feedbacks in General Circulation Models (GCMs) have been the subject of intensive study for the last four decades [*e.g., Randall et al*., 2007]. These feedbacks were identified to be one of the most significant uncertainties in projecting future global warming in past IPCC (Inter-Governmental Panel for Climate Change) Assessment Reports (AR), as well as in coupled model simulations that will be used for the upcoming AR5 [*Andrews et al.,* 2012]. Despite much progress toward understanding cloud feedbacks [Bony et al., 2006], however, there is still a general lack of knowledge about their mechanisms. Understanding the physical mechanisms is necessary to increase our confidence in the sensitivity estimates of climate models.

Cloud-climate feedbacks refer to the radiative impact of changes of clouds on climate change. Because clouds are not explicitly resolved in GCMs, they are the product of an interactive and elaborate suite of physical parameterizations. As a result, it has been a challenge to decipher cloud feedback mechanisms in climate models. Clouds also interact with the resolved-scale atmospheric dynamical circulations through their impact on latent and radiative heating.

In view of the challenges, CFMIP (the Cloud Feedback Model Intercomparison Project) and GASS (GEWEX - Global Energy and Water Cycle Experiment - Atmospheric System Study) initiated a joint project -- CGILS (the CFMIP-GASS Intercomparison of Large Eddy Models (LESs) and Single Column Models (SCMs)) to analyze the physical mechanisms of cloud feedbacks by using an idealized experimental setup. The focus of CGILS is on low clouds in the subtropics, because several studies have demonstrated that these clouds contribute significantly to cloud feedback differences in models [*e.g., Bony and Dufresne*, 2005; *Zelinka et al.,* 2012]. The role played by these

clouds is consistent with the fact that low clouds have the largest net cloud radiative effect, in contrast to deep clouds in which the positive longwave and negative shortwave cloud effects largely cancel out [*e.g. Ramanathan et al*., 1989].

The objective of this paper is to describe the CGILS project and results from 15 SCMs and eight LES models. Section 2 briefly describes the experimental design and large-scale forcing data. Section 3 gives a brief description of the participating models. Section 4 discusses simulated clouds and the associated physical processes. Section 5 presents cloud feedback results. The last section is a brief summary.

2. Experimental Design and Large-Scale Forcing Data

a. Experimental design

The CGILS experimental design was described in *Zhang et al.* [2012], which is schematically shown in Figure 1. In the control climate (CTL), sea surface temperature (SST) is specified along the GCSS/WGNE Pacific Cross Section Intercomparison (GPCI) [*Teixeira et al.*, 2011] in the northeast Pacific by using the ECMWF (European Center for Medium-Range Weather Forecasts) Interim Reanalysis (ERA-Interim) [*Dee et al.*, 2011]. In the perturbed climate, SST is uniformly raised everywhere by 2 degrees as in *Cess et al.* [1990]. Large-scale horizontal advection and vertical motion, corresponding to the underlying SST, are derived and used to force SCMs and LES models. The perturbed climate is referred to as P2S, with "S" denotes interactive large-scale subsidence with SST [*Bretherton et al.*, 2013]. The models simulate changes of clouds in response to changes of SST and the associated large-scale atmospheric conditions.

Three locations along the GPCI cross section are selected for study. They are labeled as S6, S11 and S12 in Figure 2, which also shows the distribution of low cloud amount in the summer (JJA, June to August) from the merged CALIPSO, CloudSat, CERES, and MODIS satellite product C3M [*Kato et al.* 2011; *Xu and Cheng*, 2013]. Typical regimes of clouds at these three locations are shallow cumulus (S6), cumulus under or above stratocumulus (S11), and well-mixed stratocumulus or coastal stratus (S12). On the basis of dominant cloud types, they are referred to as shallow cumulus, stratocumulus, and coastal stratus respectively. Table 1 gives the locations and values of summer-time surface meteorological variables in the control climate taken from the ERA-Interim.

b. Forcing data

The SCM and LES forcing data refer to the large-scale horizontal advective tendencies and vertical velocity, and surface boundary conditions that are specified in the model simulations. The SCMs calculate the time evolution of water vapor and temperature as follows [*Randall and Cripe*, 1999]:

$$\frac{\partial \theta_m}{\partial t} = \left(\frac{\partial \theta_m}{\partial t}\right)_{phy} - (\vec{V} \cdot \nabla \theta)_{LS} - \omega_{LS} \frac{\partial \theta_m}{\partial p} \tag{1}$$

$$\frac{\partial q_m}{\partial t} = \left(\frac{\partial q_m}{\partial t}\right)_{phy} - (\vec{V} \cdot \nabla q)_{LS} - \omega_{LS} \frac{\partial q_m}{\partial p} \quad , \tag{2}$$

where θ and q are potential temperature and water vapor mixing ratio. Subscript "m" denotes model calculations; "*LS*" stands for large-scale; other symbols are as commonly used. The first term on the right-hand-side (rhs) of Equations (1)-(2) is calculated from physical parameterizations (with subscript "*phys*"). The last two terms contain the specified large-scale horizontal advective forcing

and subsidence. In LES models, conservative variables like liquid water potential temperature and total liquid water are typically used as prognostic fields [*e.g., Siebesma et al*., 2004; *Stevens et al.,* 2005]. Equations (1) and (2) represent domain averages. The atmospheric winds and initial relative humidity are specified by using the ERA-Interim for July 2003. Initial profiles of atmospheric temperature are assumed to follow moist adiabat over the warm pool and weak gradient approximations at other locations [*Sobel et al.,* 2001]. Surface latent and sensible heat fluxes are calculated internally by each model from the specified SST and winds.

The large-scale horizontal advective tendencies and subsidence in (1)-(2) are specified according to SST. In the free troposphere, they are derived based on the clear-sky thermodynamic and water vapor mass continuity equations, in which radiative cooling in the thermodynamic equation is balanced by subsidence warming and horizontal advection, with the radiative cooling calculated by using the RRTM radiation code [*Mlawer et al.,* 1997]. Below the altitude of 900 hPa, the horizontal advective forcing of temperature and water vapor are calculated using the SST spatial gradient and specified surface relative humidity. The detailed derivation of the CGILS forcing data and its comparison with the corresponding GCM and ERA-Interim can be found in *Zhang et al*. [2012].

Figure 3a shows the derived vertical profiles of ω_{LS} in CGILS CTL (solid lines) and ERA-Interim (dashed lines) at the three chosen locations. The obtained values match well with ERA-Interim in the lower troposphere. Among the three locations, the subsidence rate is the strongest at S12 and the weakest at S6.

Figure 3b shows the comparison of the derived ω_{LS} between CTL (solid lines) and P2S (dashed lines) used in the simulations. It is seen that subsidence is weaker in the warmer climate. Figures 3c and 3d show the corresponding profiles of horizontal advective tendencies of temperature

and water vapor respectively. In the free troposphere, these profiles, along with the profiles of ω_{LS}, SST, and initial atmospheric temperature and water vapor, satisfy the clear-sky atmospheric thermodynamic and water vapor mass continuity equations under July 15 insolation conditions. *Zhang et al*. [2012] showed that the changes in the forcing data between CTL and P2S in Figure 3 capture the essential features in GCMs. All data are available in the CGILS website http://atmgcm.msrc.sunysb.edu/cfmip_figs/Case_specification.html.

c. Simulations

We use the change of cloud-radiative forcing (CRF) [*Ramanathan et al.,* 1989] from CTL to P2S, as in many previous studies, to measure cloud feedbacks. Even though *Soden et al.* [2004] suggested other better diagnostics of cloud feedbacks, CRF is used for simplicity, which should not affect the results of this paper.

The SCMs and LES are integrated to quasi-equilibrium states by using the same steady large-scale advective tendencies and subsidence as forcing data. Each model ran six simulations: CTL and P2S at the three locations of S6, S11 and S12. Since the forcing is fixed, a model may eventually drift if its radiative cooling rate in the free atmosphere differs from the rate used in the derivation of the prescribed large-scale subsidence. To prevent models from similar drifting, at pressure less than 600 hPa, temperature and water vapor mixing ratio are relaxed to their initial conditions with a time scale of 3 hours. In LES models, they are relaxed at altitudes above 4000 m for S6, 2500 m for S11, and 1200 m for S12, respectively to reduce computational costs and allow for high vertical resolutions in shallow domains. Some LES models did not complete all six simulations.

Most of the SCMs are integrated for 100 days. Based on a visual inspection of statistical equilibrium, the averages of their last period of about 50 days are used. Most LES simulations reached quasi-equilibrium states after 10 days, in which case the last two days are used in the analysis. *Zhang and Bretherton* [2008] analyzed the transient behavior of the Community Atmospheric Model (CAM) under constant forcing and showed that the interaction of different physical parameterization components can create quasi-periodic behaviors of model simulation with time scales longer than a day. Since LES models contain fewer parameterization components, the impact of this type of interactions is reduced, which may explain why LES models reach quasi-steady states in shorter time than SCMs. To our knowledge, CGILS is the first LES intercomparion study to investigate clouds by integrating them to quasi-equilibrium states.

3. Models and Differences in Physical Parameterizations

Fifteen SCMs and eight LES models participated in this study. Many parent GCMs of the SCMs also participated in the Coupled Model Intercomparison Project 5 (CMIP5). Table 2 lists the model names, main references, and CGILS contributors. It also gives the number of total vertical model layers and number of layers between the surface and 700 hPa in SCMs. The SCM vertical resolution in the boundary layer (PBL) is generally not sufficient to resolve observed thin clouds. No attempt is made to make them finer since our objective is to understand the behavior of operational GCMs. For the LES models, however, because they are intended as benchmarks, much higher resolutions are used. The horizontal resolutions of LES models are 100 meter, 50 meter and 25 meter respectively at S6, S11 and S12. The vertical resolutions of the majority of LES are 40 meter, 5 meter and 5 meter respectively at the three locations. More detailed descriptions of the CGILS LES models are given in a recent paper by *Blossey et al.* [2013].

196 The physical parameterizations in the SCMs relevant to the present study are the PBL, shallow
197 convection, and cloud schemes. For PBL schemes, the generic form can be written in terms of
198 turbulent flux at the model interfaces:

199 $$\overline{w'S'} = -K_c\left(\frac{\partial S}{\partial z} - \gamma_c\right) \quad (3)$$

200 where z is height; w is vertical velocity; S is a conservative model prognostic variable. Prime
201 represents the turbulent perturbation from the mean that is denoted by the overbar. K_c is the eddy
202 diffusivity, and γ_c is the counter-gradient transport term. In addition to resolution, the differences
203 in PBL schemes among the models are in their formulations of K_c and γ_c. For K_c, some models
204 parameterize it by using local variables at the resolved scales, such as local Richardson number in the
205 so-called first order closure models, or local turbulent eddy kinetic energy (TKE) [*Mellor and*
206 *Yamada*, 1974]. Other models use non-local empirical parameterization of K_c as a function of height
207 relative to the boundary-layer depth. Another K_c difference among the models is its parameterization
208 at the top of the PBL. While some models have explicit parameterizations of turbulent entrainment
209 based on parameters such as cloud-top radiative and evaporative cooling, others do not consider
210 entrainment. For the counter-gradient term γ_c, some models calculate it based on surface buoyancy
211 fluxes, while others do not have this term. Table 3 categorizes the PBL schemes in the SCMs
212 according to the above attributes. Cloud-top entrainment in Table 3 refers to explicit
213 parameterization. PBL schemes formulated using moist conservation variable and TKE closure (such
214 as ECHAM6) may implicitly contain cloud-top entrainment. As can be seen, a wide variety of PBL
215 parameterizations are used in the SCMs. Because of coarse vertical resolutions, however, some of

these differences do not make as much of an impact on cloud simulations as they would if higher vertical resolutions were used.

The majority of SCMs used mass-flux shallow convection schemes. The generic form of convective transport for a conservative variable *S* in these schemes is

$$\overline{w'S'} = M(z)(S_c - S_e) \tag{4}$$

where the prime denotes deviation of the bulk properties of clouds from the mean; *M* is the convective mass flux; subscripts *c* and *e* represent values in the parameterized cloud model and in the environment air respectively. The convective mass flux is calculated from parameterized rates of entrainment λ and detrainment δ:

$$\frac{1}{M}\frac{\partial M}{\partial z} = \lambda - \delta . \tag{5}$$

Some models do not separately parameterize shallow and deep convection, but because CGILS uses large-scale subsidence as forcing data, their convection schemes also simulate shallow convection. The schemes can differ in their entrainment and detrainment rates, the closure that determines the amount of cloud base mass flux, and convection triggering condition as well as origination level of convection. Table 4 categorizes the convective schemes in the SCMs based on these main attributes. Among the SCMs, CLUBB and RACMO use a single scheme to parameterize PBL turbulence and shallow convection.

Cloud schemes include a macrophysical and a microphysical component. Cloud macrophysical schemes parameterize cloud amount and the grid-scale rate of condensation and evaporation. These schemes can be generically described by assuming that the total water in the air,

236 q_t, obeys a probability distribution function (pdf) $P(q_t)$ within a model grid box. The cloud

237 amount is then

238 $$C = \int_{q_s}^{\infty} P(X)dX. \quad (5)$$

239 where q_s is the saturation vapor pressure at cloud temperature. Cloud liquid water q_l is then

240 $$q_l = \int_{q_s}^{\infty} (X - q_s)P(X)dX. \quad (6)$$

241 Therefore, cloud fraction and cloud liquid water are often proportional to each other in individual

242 models when the cloud fraction is less than 100%. The cloud microphysics scheme treats how

243 condensed water is converted to precipitation. Models differ in their assumptions on the pdf of q_t,

244 and number of hydrometer types as well as their conversion rates. Even though clouds are the

245 subject of this study, cloud schemes actually play a secondary role in inter-model differences of

246 simulated clouds in CGILS. They are not categorized here.

247 **4. Simulated Clouds and Associated Physical Processes**

248 Before investigating cloud feedbacks, we first examine the simulated clouds in CTL. Figure 4

249 shows the time-averaged cloud profiles in all 15 SCMs and all LES models, with the shallow cumulus

250 location S6 in the top row and the stratus location S12 in the bottom row. SCMs results are in the left

251 column; LES models in the middle column; observations from C3M for the summers of 2006 to 2009

252 in the right column. Note that the observations may have categorized drizzle as clouds, therefore

253 having a different definition of clouds from that in the models. The blue lines denote the ensemble

averages or multi-year averages; the red lines denote the 25 and 75 percentiles. Figure 5 shows examples of the time-pressure cross sections of these cloud amount from a sample of three SCMs (JAM, CAM4, GISS), which are selected because they span the range of model differences as will be shown later, and from one LES (SAMA).

Despite large differences among the models, they generally simulated the correct difference of cloud types from shallow cumulus, stratocumulus, and coastal stratus at the three forcing locations. The spread in the LES models is much smaller than that among the SCMs. At S11, LES models simulated shallow cumulus under stratocumulus. The use of the steady forcing for all models may have amplified the inter-model differences, since in both GCMs and the real atmosphere the large scale circulation can respond to local differences in the inversion height by partially compensating them [*Blossey et al*., 2009; *Bretherton et al*., 2013].

We find it instructive to use the following moisture budget equation to probe the physical parameterizations responsible for the simulated clouds in the SCMs. It is written as:

$$\frac{\partial q_v}{\partial t} = \left(\frac{\partial q_v}{\partial t}\right)_{turb} + \left(\frac{\partial q_v}{\partial t}\right)_{conv} - (c-e)_{stra} - [(\vec{V}\cdot\nabla q)_{LS} + \omega_{LS}\frac{\partial q_v}{\partial p}] \qquad (7)$$

where the variables are as commonly used, and the tendency terms have been separated into three physical terms representing parameterizations of PBL turbulence (*turb*), convection (*conv*), large-scale stratiform net condensation (*c*-*e*), plus the 3-dimensional large-scale forcing. As will be shown later, the separation of the physical tendency terms helps to provide a framework of interpreting cloud feedback behaviors in the models. Figure 6 shows the time averaged profiles of these three terms for the selected SCMs at S11 in CTL. The dashed lines are the simulated cloud liquid water. The solid dots on top of the dashed lines donate the mid-point of model layer.

In the JMA model, only two physical terms are active (Figure 6a). The PBL scheme moistens the boundary layer; the large-scale condensation dries it. The residual is balanced by the drying from the large-scale forcing. The peak altitudes of the "*turb*" and "*c-e*" are the same as that of the cloud liquid water. Since the PBL scheme is always active, the stratiform condensation scheme responds to the PBL scheme. In CAM4, Figure 6b shows that shallow convection is active in addition to the "*turb*" and the "*c-e*" terms. The shallow convective scheme transports the moisture from the boundary layer to the free troposphere. In the GISS model, Figure 6c shows that shallow convection is also active, but unlike CAM4, the maximum drying of the "*conv*" term is at the same level as the maximum level of "*turb*", in the middle of the cloud layer. These differences will be shown later as causes of different cloud feedbacks in the models. In Figure 6, the stratiform condensation term is the direct source of cloud water.

The inter-model differences in Figure 6 are examples of how different parameterization assumptions can affect the balance of the physical processes and associated clouds. The JMA model used the relaxed Arakawa-Schubert convection scheme [*Moorthi,* 1992] with a specified minimum entrainment for convective plumes [*Kawai*, 2012]. As a result, convection is not easily triggered in this model. CAM4 and GISS both used positive Convective Available Potential Energy (CAPE) of undiluted air parcels as criteria of convection. As a result, shallow convection is more easily triggered in these two models. Nevertheless, the assumptions in their shallow convection parameterizations are different. For example, CAM4 does not include lateral entrainment into the convective plumes [*Hack*, 1994],while GISS uses a specified value of lateral entrainment [*Del Genio and Yao,* 1993]. The shapes of the moisture tendency due to the convection schemes in the two models reflect these different assumptions. They result in the different clouds shown in Figure 4.

297 Figure 6 reminds us again the inadequate vertical resolution of SCMs in simulating the intended
298 physical processes of convection and turbulence, and so the challenge of physical parameterizations.

299 **5. Cloud Feedbacks**

300 ***a. SCM results at S11 (stratocumulus)***

301 We first use the stratocumulus regime S11 to establish a framework to interpret the cloud
302 feedbacks in the 15 SCMs. Figure 7 shows the change of net CRF from CTL to P2S at S11.
303 Increase of CRF in the figure means positive cloud feedbacks; decrease of CRF means negative
304 feedbacks. For simplicity, the change of CRF is referred to as cloud feedback. The 15 SCMs
305 simulated negative and positive cloud feedbacks that span a rather wide range. Because of the
306 simplified CGILS setup, we do not expect the feedbacks here to be the same as in the full GCMs, but
307 they allow us to gain some insight into the physical processes that determine them.

308 In Figure 7, the character "X" above a model's name indicates that shallow convection is not
309 triggered in both the CTL and P2S simulations of this model. The character "O" above a model's
310 name indicates that shallow convection is active in at least one of the simulations of CTL and P2S.
311 PBL schemes are always triggered in all models. Models without these characters about their names
312 used unified schemes of turbulence and shallow convection (such as CLUBB and RACMO) or did not
313 submit information for convection (such as ECMWF). One can see that models without shallow
314 convection tend to simulate negative cloud feedbacks, while models with active convection tend to
315 simulate positive cloud feedbacks.

316 Without convection, as discussed above for the JMA model, the water vapor balance is
317 achieved by a competition between the moistening effect of the "*turb*" term in (7) and drying effect of

318 the net large-scale condensation "*c*-*e*" term and large-scale forcing; clouds are caused by the
319 moistening term from the PBL scheme. Therefore, the response of the PBL scheme to SST largely
320 determines the change of cloud water, hence, the cloud feedbacks.

321 The PBL moistening term at the altitude of maximum cloud liquid water is larger in the
322 warmer climate in virtually all models as shown in Figure 8a. In the one exception of the CCC model,
323 the simulated altitude of maximum cloud water in P2S is much higher than in CTL, above the top of
324 the boundary layer (not shown), where the turbulent term is small.

325 The increased moistening by the PBL schemes is generally consistent with the increase of
326 surface latent heat flux (LHF) in P2S, as shown in Figure 8b. The increase of latent heat flux with
327 SST is consistent with CGILS LES simulations in *Blossey et al*. [2013] (their Table 4) and in earlier
328 LES studies under similar experimental setup [*e.g. Xu et al*., 2010]. Also, *Liepert and Previdi* [2012]
329 showed that in virtually all 21th Century climate change simulations by CMIP3 models, surface latent
330 heat fluxes are larger in a warmer climate over the oceans (their Table 2, column 3).

331 Therefore, we can use Figure 9a to conceptually summarize the main physical processes
332 responsible for negative cloud feedbacks in models without shallow convection. In these models, the
333 warmer climate has greater surface latent heat flux, larger turbulence moisture convergence in the
334 cloud layer, and consequently an inclination to give the negative cloud feedbacks. This behavior is
335 similar to the behavior of mixed layer models (MLM), which also have negative cloud feedbacks
336 [*Caldwell and Bretherton*, 2009; *Caldwell et al.,* 2013]. There are a few exceptions in which the
337 convective scheme is not active in a model, but it has small positive cloud feedbacks, such as in
338 CAM5 and ECHAM6. These may be related with cloud-top entrainment, included explicitly and
339 implicitly in these models, that acts like shallow convection.

We now turn to models with active shallow convection. Figure 7 shows that these models tend to have positive cloud feedbacks. As discussed in the previous section for CAM4 and GISS, shallow convection acts to dry the cloud layer. It is a moisture sink that has the same sign as the stratiform condensation sink in equation (7). The enhanced moistening from the PBL scheme in the warmer climate is approximately balanced by enhanced drying from the sum of the stratiform condensation and shallow convection. When the rate of drying from the shallow convection is greater than the rate of moistening from the PBL scheme as SST increases, the stratiform condensation can decrease in a warmer climate. This tends to reduce cloud water and clouds, thus causing positive cloud feedback.

The enhanced rate of convective drying in the warmer climate may be explained by looking at the moisture flux in equation (4) immediately above the top of the boundary layer. The convective transport of total water out of the top of boundary-layer clouds depends on the moisture contrast across the cloud top and the convective mass flux. The moisture contrast is larger in the warmer climate, since the subsiding free tropospheric air remains dry but the total water in convective plumes increases with SST. The convective mass fluxes of shallow convection, for reasons unknown to us, generally increase in the warmer climate (not shown), which is different from the change of mass flux of deep convection [*Held and Soden*, 2006]. The role of active convection therefore tends to cause decrease of clouds and positive cloud feedbacks.

We use Figure 9b as a schematic of the positive cloud feedbacks in the models. We can interpret the net cloud feedbacks as due to two opposing roles of surface-based PBL turbulence and shallow convection, with the latter dominating in most of the models in which convection is active. Figure 9b also applies to models with parameterizations of significant cloud-top entrainment. The

362 PBL scheme can also be dominant over the shallow convection scheme in some models, such as in
363 CAM4. In this model, as discussed in the previous section, the peak drying of shallow convection
364 occurs below the cloud layer instead of within the cloud layer.

365 Why does shallow convection tend to play the dominant role in determining the net cloud
366 feedback in the models? We offer a plausible explanation here. If the convective mass flux does not
367 change, the upward moisture flux immediately above the PBL cloud top described in (4) should
368 change with SST approximately at the rate of the Clausius-Clapeyron relationship (7% per degree).
369 This flux is a measure of the convective drying of the cloud layer. The surface latent heat flux, on the
370 other hand, generally increases with SST at a smaller rate of about 3% calculated from Figure 8b,
371 which is also consistent with previous studies [*e.g., Held and Soden*, 2006]. This flux is a measure of
372 moistening by the PBL scheme. The net effect therefore tends to be dominated by that of convection.
373 *Brient and Bony* [2012] used the larger moisture contrast between the free troposphere and boundary
374 layer in the warmer climate to explain the positive cloud feedbacks in the LMD SCM and GCM; while
375 *Kawai* [2012] used the increased surface flux to explain the negative cloud feedback in the JMA SCM
376 and GCM. These are consistent with the present interpretation. In GCMs or in the real atmospheres,
377 any changes in the frequency of convection and convective mass fluxes would also matter.

378 We need to point out that the separation of the effects of PBL turbulence and shallow
379 convection in the framework of Figure 9 is an artifact of the GCMs. However, this is what the current
380 generation of climate models used.

381 ***b. SCM results at S6 (shallow cumulus) and at S12 (coastal stratus)***

382 We now use the same framework as we used for S11 to interpret SCMs results at the other two
383 locations. Before proceeding, we need to supplement our schematics with another scenario in which
384 the depth of convection is large and mixing of cloudy air with dry air can occur laterally. If the
385 cloud-scale dynamical fields are the same, larger drying is expected in P2S than CTL because of the
386 larger moisture contrast across cloud boundaries. This is schematically shown in Figure 9c. Other
387 factors such as cloud-scale dynamics, cloud depth, and cloud microphysics can also change in a
388 warmer climate, leading to more complicated behavior of cloud feedbacks. This scenario also
389 includes regime change of clouds from stratocumulus to shallow cumulus as exhibited by some
390 models (e.g., CCC at S11, not shown).

391 Figure 10a shows the SCM cloud feedbacks at the shallow convection location S6. The
392 models are ordered in the same sequence as in Figure 7. Almost all models simulated convection at
393 S6. Partially due to the complications described above, convection at S6 does not necessarily
394 correspond to positive cloud feedbacks. In all simulations, surface latent heat flux is greater in the
395 warmer climate (not shown). We may therefore use the same framework as for S11 to think that the
396 larger surface latent heat flux alone is a factor for more clouds in a warmer climate, but the other
397 factors from shallow convection such as lateral mixing favor more dilution of clouds and a positive
398 cloud feedback. The two effects compensate each other differently in the models because of the
399 different assumptions in the specific parameterizations.

400 Figure 10b shows SCM results at S12, where SST is colder and subsidence is stronger than at
401 S11. Clouds are restricted to within the boundary layer. The simulated cloud feedbacks also span a
402 wide range. Three models simulated no clouds at this location (GFDL AM3, EC-ETH, CAM5) (due
403 to the constancy of forcing). Most models simulated the same cloud feedback signs as at S11. Some

simulated opposite signs, one of which is the GISS model. As indicated by the "X" character above the GISS model in Figure 10b, for this model, shallow convection is not active at S12, in contrast to be active at S11. Therefore, the cloud feedback changed sign. In all models except for ACCESS, surface latent heat flux is larger in P2S at S12 (not shown). The conceptual framework in Figures 9a and 9b can be generally applied to describe the behavior of cloud feedbacks in the SCMs at S12

c. LES results

To compare with SCM results, in Figures 11a to 11c, we show the LES cloud feedbacks at the three locations of S6, S11 and S12 respectively. The LES results are more consistent with each other than SCMs. At the shallow cumulus location S6 (Figure 11a), LES models simulated a small positive cloud feedback except for DALES and WRF that had negligible feedbacks. At the stratocumulus location S11 (Figure 11b), all models except for SAM simulated positive cloud feedbacks. At the coastal stratus location S12 (Figure 11c), all except for DALES simulated positive cloud feedback.

There is therefore consensus, but not uniform agreement, among the LES models with regard to simulated cloud feedbacks. The LES results tend to support the framework we proposed in Figure 9: In regimes where the PBL is relatively well mixed, cloud feedback is negative, while in regimes where shallow convection is active, cloud feedback tends to be positive.

Detailed analyses of the LES turbulence and cloud simulations from the CGILS experiments have been described in *Blossey et al.* [2013]. A companion paper by Bretherton et al. [2013] investigated the sensitivity of LES results to large-scale conditions. We point out that the consensus among the LES model does not necessarily mean they simulated the correct cloud feedbacks.

Nevertheless they give plausible answers for SCMs to target for. Eventually, they need to be validated by observations under more realistic experimental setups.

6. Summary and Discussion

The experimental setup of CGILS was used to simulate shallow cumulus, startocumulus and coastal stratus and to investigate the physical mechanisms of cloud feedbacks under idealized climate change. In models where shallow convection is not activated or plays minor role in drying the cloud layer, cloud feedbacks tend to be negative. In models when convection is active, cloud feedbacks tend to be positive in the stratocumulus and coastal stratus regime, but uncertain in the shallow cumulus regime. A framework is described to interpret the SCM cloud feedbacks by using the two opposing effects of increased moistening from PBL scheme and drying from the convection in a warmer climate, with the PBL schemes causing negative cloud feedbacks while the convective schemes causing positive cloud feedbacks. The convective scheme plays a more dominant role at times when it is active, which is explained by using the relative change of the moisture contrasts between the cloud layer and surface and between the cloud layer and the free troposphere.

LES models simulated overall consistent positive cloud feedbacks in the shallow cumulus and stratocumulus regimes, but negative feedbacks in the coastal stratus regime. The same framework used to interpret the SCM cloud feedbacks is applicable to the LES results.

The relevance of CGILS results to cloud feedbacks in GCMs and in real-world climate changes is not clear yet. Several recent works have started to address this question [*Brient and Bony*, 2012; *Kawai*, 2012; *Webb and Lock, 2012*]. CGILS results have provided us insights into low cloud feedbacks in models regardless of its simple idealized set up. It is hoped that these physical

445 understandings can eventually help to reduce the cloud feedback uncertainties in models. For
446 example, because of the opposing roles of the turbulence scheme and shallow convection scheme in
447 causing cloud feedbacks in the models, it is desirable to parameterize these two related processes as a
448 single system rather than as separate model components.

449

Acknowledgements

Sing-bin Park of the Seoul National University (SNU) participated in the initial phase of the CGILS project. His tragic death disrupted the submission of results from the SNU model. This paper serves as an appreciation and memory of him. Zhang's CGILS research is supported by the Biological and Environmental Research Division in the Office of Sciences of the US Department of Energy (DOE) through its FASTER project, by the NASA Modeling and Analysis Program (MAP) and the US National Science Foundation to the Stony Brook University. Bretherton and Blossey acknowledge support from the NSF Center for Multiscale Modeling and Prediction, Austin is supported by Canada's NSERC,. Del Genio is supported by the NASA MAP program. V. Larson gratefully acknowledges support from the National Science Foundation (grant AGS-0968640) and the U. S. Department of Energy (grant DE-SC0006927). Wolf was supported by the DOE ASR program. Webb was supported by the Joint DECC/Defra Met Office Hadley Centre Climate Programme (GA01101) and funding from the European Union, Seventh Framework Programme (FP7/2007-2013) under grant agreement number 244067 via the EU CLoud Intercomparison and Process Study Evaluation Project (EUCLIPSE). Franklin was supported by the Australian Climate Change Science Program, funded jointly by the Department of Climate Change and Energy Efficiency, the Bureau of Meteorology and CSIRO. Heus was funded by the Deutscher Wetter Dienst (DWD) through the Hans-Ertel Centre for Weather Research, as part of the EUCLIPSE project under Framework Program 7 of the European Union. The simulations with the Dutch LES model were sponsored by the National Computing Facilities Foundation (NCF). The National Center for Atmospheric Research is sponsored by the National Science Foundation.

REFERENCES

Andrews, T., J. M. Gregory, M. J. Webb, and K. E. Taylor (2012), Forcing, feedbacks and cli- mate sensitivity in CMIP5 coupled atmosphere-ocean climate models, *Geophys. Res. Lett.* 39, doi:10.1029/2012GL051607.

Blossey, P. N., C. S. Bretherton, M. Zhang, A. Cheng, S. Endo, T. Heus, Y. Liu, A. Lock, S. R. de Roode and K.-M. Xu (2013). Marine low cloud sensitivity to an idealized climate change: The CGILS LES Intercomparison, *J. Adv. Model. Earth Syst.*, doi:10.1002/jame.20025.

Blossey, P. N., C. S. Bretherton, and M. C. Wyant (2009), Understanding subtropical low cloud response to a warmer climate in a superparameterized climate model. Part II: Column modeling with a cloud-resolving model, *Journal of Advancing Modeling Earth Systems*, 1, Art. #8, 14 pp., doi:10.3894/JAMES.2009.1.8.

Bretherton, C. S., P. N. Blossey, C. R. Jones (2013), A Large-Eddy Simulation of Mechanisms of Boundary Layer Cloud Response to Climate Change in CGILS, *Journal of Advances in Modeling Earth Systems.* doi:10.1002/jame.20019.

Bretherton, Christopher S., Sungsu Park (2009), A New Moist Turbulence Parameterization in the Community Atmosphere Model, *J. Climate*, 22, 3422–3448. doi: http://dx.doi.org/10.1175/2008JCLI2556.1

Brinkop, S., E. Roeckner (1995), Sensitivity of a General Circulation Model to Parameterizations of Cloud–Turbulence Interactions in the Atmospheric Boundary Layer, Tellus 47A: pp. 197-220.

Bony, S., and J.-L. Dufresne (2005), Marine boundary layer clouds at the heart of cloud feedback uncertainties in climate models, *Geophys. Res. Lett.*, 32, L20806, doi:10.1029/2005GL023851.

Bony, Sandrine, Kerry A. Emanuel (2005), On the Role of Moist Processes in Tropical Intraseasonal Variability: Cloud–Radiation and Moisture–Convection Feedbacks, J. Atmos. Sci., 62, 2770–2789. doi: http://dx.doi.org/10.1175/JAS3506.1

Bony, S., and coauthors (2006), How well do we understand climate change feedback processes? *J. Climate*, 19, 3445-3482.

Brient, F., and S. Bony (2012), Interpretation of the positive low cloud feedback predicted by a climate model under global warming, Clim. Dyn., doi:10.1007/s00382-011-1279-7.

Caldwell, P., and C. S. Bretherton (2009), Response of a subtropical stratocumulus-capped mixed layer to climate and aerosol changes, *J. Climate*, 22, 20-38.

Caldwell, P. M., Y. Zhang, and S. A. Klein (2013), CMIP3 subtropical stratocumulus cloud feedback interpreted through a mixed-layer model, J. Climate, **26**, 1607–1625. doi: http://dx.doi.org/10.1175/JCLI-D-12-00188.1

Cess, R. D, and Coauthors (1990), Intercomparison and interpretation of cloud-climate feedback processes in nineteen atmospheric general circulation models, *J. Geophys. Res.*, 95, 16 601–16 615.

Dee, D. P., and coauthors (2011), The ERA-Interim reanalysis: configuration and performance of the data assimilation system, *Quart. J. Roy. Meteor. Soc.*, 137, 553-597. DOI: 10.1002/qj.828

Del Genio, A. D., and M. Yao (1993), Efficient cumulus parameterization for long-term climate studies: The GISS scheme, in The Representation of Cumulus Convection in Numerical Models, Meteorol. Monogr., 46, 181–184.

Donner, Leo J., and Coauthors (2011), The Dynamical Core, Physical Parameterizations, and Basic Simulation Characteristics of the Atmospheric Component AM3 of the GFDL Global Coupled Model CM3, *J. Climate*, 24, 3484–3519. doi: http://dx.doi.org/10.1175/2011JCLI3955.1

518 Emanuel, A. Kerry (1991), A Scheme for Representing Cumulus Convection in Large-Scale Models,
519 *J. Atmos. Sci.*, 48, 2313–2329. doi: http://dx.doi.org/10.1175/1520-
520 0469(1991)048<2313:ASFRCC>2.0.CO;2
521 Endo, S., Y. Liu, W. Lin, and G. Liu, G (2013), Extension of WRF to Cloud-Resolving Simulations
522 Driven by Large-Scale and Surface Forcings. Part I: Model Configuration and Validation,
523 Mon. Weather Rev., submitted. (BNL-96480-2011-JA) Available at
524 http://www.bnl.gov/envsci/pubs/pdf/2013/BNL-96480-2011-JA.pdf.
525 Golaz, Jean-Christophe, Vincent E. Larson, William R. Cotton (2002a), A PDF-Based Model for
526 Boundary Layer Clouds. Part I: Method and Model Description, *J. Atmos. Sci.*, 59, 3540–3551.
527 doi: , http://dx.doi.org/10.1175/1520-0469(2002)059<3540:APBMFB>2.0.CO;2
528 Golaz, Jean-Christophe, Vincent E. Larson, William R. Cotton (2002b), A PDF-Based Model for
529 Boundary Layer Clouds. Part I: Method and Model Description, *J. Atmos. Sci.*, 59, 3540–3551.
530 doi: http://dx.doi.org/10.1175/1520-0469(2002)059<3540:APBMFB>2.0.CO;2
531 Golaz, Jean-Christophe, Vincent E. Larson, James A. Hansen, David P. Schanen, Brian M. Griffin
532 (2007), Elucidating Model Inadequacies in a Cloud Parameterization by Use of an Ensemble-
533 Based Calibration Framework, *Mon. Wea. Rev.*, 135, 4077–4096. doi:
534 http://dx.doi.org/10.1175/2007MWR2008.1
535 Grant, A. L. M. (2001), Cloud-base fluxes in the cumulus-capped boundary layer, *Quart. J. Roy.*
536 *Meteor. Soc.*, 127, 407–421.
537 Gregory, D., and P. R. R. Rowntree (1990), A mass flux convection scheme with representation of
538 cloud ensemble characteristics and stability dependent closure, Mon.Wea. Rev., 118, 1483
539 1506.

Hack, J. J. (1994), Parameterization of moist convection in the National Center for Atmospheric Research community climate model (CCM2), J. Geophys. Res., 99, 5551-5568.

Held, Isaac M., Brian J. Soden (2006), Robust Responses of the Hydrological Cycle to Global Warming, *J. Climate*, 19, 5686–5699. Doi http://dx.doi.org.libproxy.cc.stonybrook.edu/10.1175/JCLI3990.1

Heus, T., C.C. van Heerwaarden, H.J.J. Jonker, A.P. Siebesma, S. Axelsen, K. van den Dries, O. Geoffroy, A.F. Moene, D. Pino, S.R. de Roode and J. Vila-Guerau de Arellano, Formulation of the Dutch Atmospheric Large-Eddy Simulation (DALES) and overview of its applications, Geoscientific Model Development (2010, 3, 415-444, doi:10.5194/gmd-3-415-2010.

Hewitt, H.T., D. Copsey, I.D. Culverwell, C.M. Harris, R.S.R. Hill, A.B. Keen, A.J. McLaren and E.C. Hunke (2011), Design and implementation of the infrastructure of HadGEM3: the next generation Met Office climate modelling system, *Geosci., Model Dev.*, 4, 223 – 253.

Holtslag, A. A. M., B. A. Boville (1993), Local Versus Nonlocal Boundary-Layer Diffusion in a Global Climate Model, *J. Climate*, 6, 1825–1842. doi: http://dx.doi.org/10.1175/1520-0442(1993)006<1825:LVNBLD>2.0.CO;2

Holtslag, A. A. M., Chin-Hoh Moeng (1991), Eddy Diffusivity and Countergradient Transport in the Convective Atmospheric Boundary Layer, *J. Atmos. Sci.*, 48, 1690–1698. doi: http://dx.doi.org/10.1175/1520-0469(1991)048<1690:EDACTI>2.0.CO;2

Hourdin, F., I. Musat, S. Bony, P. Braconnot, F. Codron, J. Dufresne, L. Fairhead, M. Filiberti, P. Friedlingstein, J. Grandpeix, G. Krinner, P. LeVan, L. Zhao-Xin, and F. Lott (2006), The LMDZ4 general circulation model: climate performance and sensitivity to parametrized physics with emphasis on tropical convection, Climate Dynamics 27(7), 787–813.

562 Isotta F.A., Spichtinger P, Lohmann U, et al. (2011), Improvement and Implementation of a
563 Parameterization for Shallow Cumulus in the Global Climate Model ECHAM5-HAM, J.
564 Atmos. Sci, 68, 515-532.
565 Kato, S., and coauthors (2011), Improvements of top-of-atmosphere and surface irradiance
566 computations with CALIPSO, CloudSat, and MODIS-derived cloud and aerosol properties, *J.*
567 *Geophys. Res.,* 116, D19209, doi:10.1029/2011JD016050.
568 Kawai, H. (2012), Examples of mechanisms for negative cloud feedback of stratocumulus and stratus
569 in cloud parameterizations, Scientific Online Letters on the Atmosphere, Vol. 8, 150−154,
570 doi:10.2151/sola.2012-037
571 Khairoutdinov, M. F., and D.A. Randall (2003), Cloud-resolving modeling of the ARM summer 1997
572 IOP: Model formulation, results, uncertainties and sensitivities, J. Atmos. Sci., 60, 607-625.
573 Larson, V. E. and J.-C. Golaz (2005), Using probability density functions to derive consistent closure
574 relationships among higher-order moments, Mon. Wea. Rev., 133, 1023–1042.
575 Liepert, B. G., and M. Previdi (2012), Inter-model variability and biases of the global water cycle in
576 CMIP3 coupled climate models, Environmental Research Letters, 7, 014006(2012),
577 doi:10.1088/1748-9326/7/1/014006.
578 Lock, A.P. (2009), Factors influencing cloud area at the capping inversion for shallow cumulus clouds,
579 Q.J.R. Meteorol. Soc., 135: 941–952. doi: 10.1002/qj.424.
580 Lock, A. P., A. R. Brown, M. R. Bush, G. M. Martin, R. N. B. Smith (2000), A New Boundary Layer
581 Mixing Scheme. Part I: Scheme Description and Single-Column Model Tests, Mon. Wea.
582 Rev., 128, 3187–3199. doi: http://dx.doi.org/10.1175/1520
583 0493(2000)128<3187:ANBLMS>2.0.CO;2

584 Louis, J. (1979), A parametric model of vertical eddy fluxes in the atmosphere, Boundary-layer
585 Meteorology - BOUND-LAY METEOROL , vol. 17, no. 2, pp. 187-202, DOI:
586 10.1007/BF00117978
587 Ma X. and K. von Salzen, Cole J. (2010), Constraints on first aerosol indirect effect from a
588 combination of MODIS-CERES satellite data and global climate simulations, Atmospheric
589 Chemistry and Physics Discussions 01/2010;
590 DOI:http://www.doaj.org/doaj?func=openurl&genre=article&issn=16807367&date=2010&vol
591 ume=10&issue=6&spage=13945
592 Martin, G. M., N. Bellouin, W. J. Collins, I. D. Culverwell and P. R. Halloran, S. C. Hardiman, T. J.
593 Hinton and C. D. Jones (2011), The HadGEM2 family of Met Office Unified Model climate
594 configurations. Geosci. Model Devel. 2011 4 723--757 10.5194/gmd-4-723-2011.
595 Medeiros B, Stevens B, Held IM, Zhao M, Williamson DL, Olson JG, Bretherton CS (2008),
596 Aquaplanets, Climate Sensitivity, and Low Clouds, J Clim 21 (19):4974–4991, DOI
597 10.1175/2008JCLI1995.1
598 Mellor, George L., Tetsuji Yamada (1974), A Hierarchy of Turbulence Closure Models for Planetary
599 Boundary Layers, *J. Atmos. Sci.*, 31, 1791–1806. doi: http://dx.doi.org/10.1175/1520-
600 0469(1974)031<1791:AHOTCM>2.0.CO;2
601 Mlawer, E.J., S.J. Taubman, P.D. Brown, M.J. Iacono and S.A. Clough (1997), RRTM, a validated
602 correlated-k model for the longwave, J. Geophys. Res., 102, 16,663-16,682.
603 Moorthi, Shrinivas, Max J. Suarez (1992), Relaxed Arakawa-Schubert. A Parameterization of Moist
604 Convection for General Circulation Models, *Mon. Wea. Rev.*, 120, 978–1002. doi:
605 http://dx.doi.org/10.1175/1520-0493(1992)120<0978:RASAPO>2.0.CO;2

606 Neale, R. B., et al. (2012), Description of the NCAR Community Atmospheric Model (CAM5.0),
607 NCAR/TN 486+STR. Available at
608 http://www.cesm.ucar.edu/models/cesm1.0/cam/docs/description/cam5_desc.pdf
609 Neale, R. B. J. Richter, S. Park, P. H. Lauritzen, S. J. Vavrus, P. J. Rasch, and M. Zhang (2013), The
610 Mean Climate of the Community Atmosphere Model (CAM4) in Forced SST and Fully
611 Coupled Experiments, *J. Climate*. Submitted.
612 Neggers, R. A. J., M. Koehler and A. A. M. Beljaars (2009a), A dual mass flux framework for
613 boundary-layer convection, Part I: Transport. J. Atmos. Sci., 66, 1465-1487,
614 doi:10.1175/2008JAS2635.1
615 Neggers, R. A. J. (2009b), A dual mass flux framework for boundary-layer convection, Part II:
616 Clouds. J. Atmos. Sci., 66, 1489-1506, doi:10.1175/2008JAS2636.1
617 Park, Sungsu, Christopher S. Bretherton (2009), The University of Washington Shallow Convection
618 and Moist Turbulence Schemes and Their Impact on Climate Simulations with the Community
619 Atmosphere Model, *J. Climate*, 22, 3449–3469. doi:
620 http://dx.doi.org/10.1175/2008JCLI2557.1
621 Ramanathan, V., R. D. Cess, E. F. Harrison, P. Minnis, B. R.Barkstrom, and D. L. Hartmann (1989),
622 Cloud-radiative forcing and climate: Results from the Earth Radiation Budget Experiment,
623 *Science,* 243, 57–63.
624 Randall, D. A., and D. G. Cripe (1999), Alternative methods for specification of observed forcing in
625 single-column models and cloud system models, *J. Geophys. Res.*, 104(D20), 24,527–24,545,
626 doi:10.1029/1999JD900765.
627 Randall, D. A., and Coauthors (2007), Climate models and their evaluation, *Climate Change 2007:*
628 *The Scientific Basis,* S. Solomon et al., Eds., Cambridge University Press, 589–662.

629 Schmidt, G.A., R. Ruedy, J.E. Hansen, I. Aleinov, N. Bell, M. Bauer, S. Bauer, B. Cairns, V. Canuto,
630 Y. Cheng, A. Del Genio, G. Faluvegi, A.D. Friend, T.M. Hall, Y. Hu, M. Kelley, N.Y. Kiang,
631 D. Koch, A.A. Lacis, J. Lerner, K.K. Lo, R.L. Miller, L. Nazarenko, V. Oinas, Ja. Perlwitz, Ju.
632 Perlwitz, D. Rind, A. Romanou, G.L. Russell, Mki. Sato, D.T. Shindell, P.H. Stone, S. Sun, N.
633 Tausnev, D. Thresher, and M.-S. Yao (2006), Present day atmospheric simulations using GISS
634 ModelE: Comparison to in-situ, satellite and reanalysis data, J. Climate, 19, 153-192.
635 Siebesma, A. P., and coauthors (2004), Cloud representation in general circulation models over the
636 northern Pacific Ocean: A EUROCS intercomparison study, *Quart. J. Roy. Meteor. Soc.*,
637 130, 3245-3267.
638 Simmons, A., S. Uppala, D. Dee, and S. Kobayashi (2007), ERA-Interim: New ECMWF reanalysis
639 products from 1989 onwards, *ECMWF Newsletter,* No. 110, ECMWF, Reading, United
640 Kingdom, 25–35.
641 Soden, B. J., and I. M. Held (2006), An assessment of climate feedbacks in coupled ocean atmosphere
642 models, *J. Climate,* 19, 3354–3360.
643 Soden, A. J. Broccoli, and R. S. Hemler (2004), On the use of cloud forcing to estimate cloud
644 feedback, *J. Climate*, 17, 3661–3665.
645 Sobel, A., Nilsson, and L. Polvani (2001), The weak temperature gradient approximation and balanced
646 tropical moisture waves, *Journal of the Atmospheric Sciences*, 58, 3650-3665.
647 Stevens, B., and coauthors (2005), Evaluation of large-eddy simulations via observations of nocturnal
648 marine stratocumulus, Mon. Wea. Rev., 133, 1443-1462.
649 Stevens, B., et al. (2013), The Atmospheric Component of the MPI-M Earth System Model:
650 ECHAM6, J. Adv. Model. Earth Syst., DOI: 10.1002/jame.20015.

Stevens, B. and A. Seifert (2008), Understanding macrophysical outcomes of microphysical choices in simulations of shallow cumulus convection, J. Meteor. Soc. Japan, vol. 86A, pp. 143-162.

Teixeira, J., and Coauthors (2011), Tropical and Subtropical Cloud Transitions in Weather and Climate Prediction Models: The GCSS/WGNE Pacific Cross-Section Intercomparison (GPCI), *J. Climate*, 24, 5223–5256. doi:http://dx.doi.org.libproxy.cc.stonybrook.edu/10.1175/2011JCLI3672.1

Tiedtke, M. (1989), A Comprehensive Mass Flux Scheme for Cumulus Parameterization in Large-Scale Models, *Mon. Wea. Rev.*, 117, 1779–1800. doi: http://dx.doi.org/10.1175/1520-0493(1989)117<1779:ACMFSF>2.0.CO;2

von Salzen, K. et al. (2013), The Canadian Fourth Generation Atmospheric Global Climate Model (CanAM4). Part I: Representation of Physical Processes. Ocean-Atmosphere, Accepted.

von Salzen, Knut, Norman A. McFarlane (2002), Parameterization of the Bulk Effects of Lateral and Cloud-Top Entrainment in Transient Shallow Cumulus Clouds, *J. Atmos. Sci.*, 59, 1405–1430. doi: http://dx.doi.org/10.1175/1520-0469(2002)059<1405:POTBEO>2.0.CO;2

Webb, M. and Coauthors (2006), On the contribution of local feedback mechanisms to the range of climate sensitivity in two GCM ensembles, *Climate Dyn.*, 27, 17–38.

Webb, M. J. and A. Lock (2012), Coupling between subtropical cloud feedback and the local hydrological cycle in a climate model, *Climate Dyn*, DOI 10.1007/s00382-012-1608-5.

Wyant, M. C., C. S. Bretherton, J. T. Bacmeister, J. T. Kiehl, I. M. Held, M. Zhao, S. A. Klein, and B. J. Soden (2006), A comparison of low-latitude cloud properties and their response to climate change in three AGCMs sorted into regimes using mid-tropospheric vertical velocity, *Climate Dyn.*, 27, 261–279, doi:10.1007/s00382-006-0138-4.

673 Xu, K.-M., and A. Cheng (2013), Evaluating low cloud simulation from an upgraded multiscale
674 modeling framework. Part II: Seasonal variations over the Eastern Pacific, *J. Climate*,
675 doi:10.1175/JCLI-D-12-00276.1.
676 Xu, K.-M., A. Cheng, and M. Zhang (2010), Cloud-resolving simulation of low-cloud feedback to an
677 increase in sea surface temperature, J. Atmos. Sci., 67, 730-748.
678 Zelinka, Mark D., Stephen A. Klein, Dennis L. Hartmann (2012), Computing and Partitioning Cloud
679 Feedbacks Using Cloud Property Histograms. Part I: Cloud Radiative Kernels, *J. Climate*, 25,
680 3715–3735. doi: http://dx.doi.org.libproxy.cc.stonybrook.edu/10.1175/JCLI-D-11-00248.1
681 Zhang, M., and C. S. Bretherton (2008), Mechanisms of low cloud climate feedback in idealized
682 single-column simulations with the Community Atmospheric Model (CAM3), *J. Climate*, 21,
683 4859-4878.
684 Zhang, M.,et al. (2012), CGILS: An experimental design to study low cloud feedbacks in general
685 circulation models by using Single-Column and Large Eddy Simulation models, Journal of
686 Advances in Modeling Earth Systems. Vol. 4, No. 4, doi:10.1029/2012MS000182.

687

688

689

690

691

692 **Tables**

693 Table 1: Study locations and surface meteorological conditions in the control climate

	S6 Shallow Cu	S11 Stratocumulus	S12 Stratus
Latitude (Degrees North)	**17^{o}N**	**32^{o}N**	**35^{o}N**
Longitude (Degrees)	**149^{o}W**	**129^{o}W**	**125^{o}W**
Sea-level pressure (mb)	**1014.1**	**1020.8**	**1018.6**
SST (^{o}C)	**25.6**	**19.3**	**17.8**
Tair_surface (^{o}C)	**24.1**	**17.8**	**16.3**
U_surface (m/s)	**-7.4**	**-1.8**	**2.1**
V_surface (m/s)	**-2.7**	**-6.5**	**-8.0**
RH_surface (m/s)	**80%**	**80%**	**80%**
Mean TOA insolation (w/m2)	**448.1**	**471.5**	**473.1**
Mean daytime solar zenith angle	**51.0**	**52.0**	**52.7**
Daytime fraction on July 15	**0.539**	**0.580**	**0.590**
Eccentricity on July 15	**0.967**	**0.967**	**0.967**
Surface Albedo	**0.07**	**0.07**	**0.07**

694
695

696 Table 2: Participating models, main references, and contributors. The number of vertical layers and

697 layers between the surface and 700 hPa for SCMs are given in the last column

Models Acronyms	Model Institution	References	Contributors	Layers: Total/ (p>700 hPa)
SCM (15)				
ACCESS (Australian Community Climate and Earth System Simulator)	Australian Commonwealth Scientific and Industrial Research Organisation/Centre for Australian Weather and Climate Research	*Hewitt et al.* [2011]	Charmaine Franklin	38/12
CAM4 (Community Atmospheric Model Version 4)	National Center for Atmospheric Research (NCAR), USA	*Neale et al.* [2013]	Minghua Zhang, Cecile Hannay, Philip Rasch	26/5
CAM5 (Community Atmospheric Model Version 4)	National Center for Atmospheric Research (NCAR), USA	*Neale et al.* [2012]	Minghua Zhang, Cecile Hannay, Philip Rasch	30/9
CCC (Canadian Centre for Climate)	Canadian Centre for Climate Modelling and Analysis, Canada	*Ma et al.* [2010]	Phillip Austin, Knut von Salzen	35/14
CLUBB (Cloud Layers Unified By Binormals)	University of Wisconsin at Milwaukee, USA	*Golaz et al.* [2002a,b], *Larson and Golaz* [2005], *Golaz et al.* [2007]	Vincent Larson, Ryan Senkbeil	41/29
ECHAM6 (ECMWF-University of Hamburg Model Version 6)	Max-Planck Institute of Meteorology, Germany	*Stevens et al.*[2013]	Suvarchal Cheedela, Bjorn Stevens	31/9
ECMWF (European Center for Medium Range Weather Forecasting)	European Center for Medium Range Weather Forecasting	*Neggers et al* [2009a; 2009b]	Martin Koehler	91/20
EC-ETH (ECMWF-Eidgenössische Technische Hochschule)	Swiss Federal Institute of Technology, Switzerland	*Isotta et al.* [2011]	Colombe Siegenthaler-Le Drian, Isotta Alessandro Francesco ,Ulrike Lohman	31/9
GFDL-AM3 (Geophysical Fluid Dynamics Laboratory Atmospheric Model Version 3)	NOAA Geophysical Fluid Dynamics Laboratory, USA	*Donner et al.* [2011]	Jean-Christophe Golaz, Ming Zhao	48/12
GISS (Goddard Institute for Space Studies)	NASA Goddard Institute for Space Studies, USA	*Schmidt et al.* [2006]	Anthony DelGenio, Audrey Wolf	40/9
GMAO	NASA Goddard Space Flight	*Bacmeister et al.*	Andrea Molod, Max	

(NASA Global Modeling and Assimilation Office)	Center, USA	[2006]	Suarez, Julio Bacmeister	27/13
HadGEM2 (Hadley Centre Global Environment Model version 2)	Met Office, United Kingdom	*Lock et al.* [2001], *Martin et al*. [2011]	Adrian Lock, Mark Webb	38/12
JMA (Japanese Meteorological Agency)	Japanese Meteorological Agency, Japan	Kawai [2012]	Hideaki Kawai	60/16
IPSL (Institute Pierre Simon Laplace)	Institute Pierre Simon Laplace (IPSL), France	*Bony and Emanuel* [2001], *Hourdin et al.* [2006]	Florent Brient, Sandrine Bony, Jean-Louis Dufresne	39/12
RACMO (Regional Atmospheric Climate Model**)**	Royal Netherlands Meteorological Institute, the Netherlands	*Neggers et al* [2009a;2009b]	Roel Neggers, Pier Siebesma	91/20
LES (8)				
DALES (Dutch Atmospheric. Large-Eddy Simulation)	Royal Netherlands Meteorological Institute, the Netherlands	*Heus et al.* [2010]	Stephan de Roode	
LARC (NASA Langley Research Center)	NASA Langley Research Center, USA	*Xu et al.* [2010]	Anning Cheng, Kuan-man Xu	
SAM (System for Atmospheric Models)	University of Washington/Stony Brook University, USA	*Khairtoutdinov and Randall* [2003]	Peter Blossey, Chris Bretherton, Marat Khairoutdinov	
SAMA (System for Atmospheric Models)	University of Washington/Stony Brook University, USA	*Khairtoutdinov and Randall* [2003], *Lock* [2009], *Blossey et al.* [2013]	Peter Blossey, Chris Bretherton, Marat Khairoutdinov	
MOLEM (Met Office Large Eddy Model)	Met Office, United Kingdom	Lock [2009]	Adrian Lock	
MOLEMA (Met Office Large Eddy Model)	Met Office, United Kingdom	*Lock* [2009], *Blossey et al.* [2013]	Adrian Lock	
UCLA (University of California at Los Angeles)	Max Plank Institute of Meteorology, Germany/University of California at Los Angeles, USA	*Stevens et al.* [2005], *Stevens and Seifert* [2008]	Thijs Heus, Irina Sandu, Bjorn Stevens	
WRF (Weather Research and Forecasting)	National Center for Atmospheric Research/Brookhaven National Laboratory	*Endo et al.* [2013]	Satosh End, Yangang Liu	

698

699
700

701

702 Table 3: Boundary-layer turbulence schemes in SCMs

Models	References	Local K_c	Cloud-top entrainment	Counter Gradient γ_c
ACCESS	*Lock et al*. [2000]	N	Y	Y
CAM4	*Holtslag and Boville* [1993]	N	N	Y
CAM5	*Bretherton & Park* [2009]	Y	Y	N
CCC	*von Salzen et al.* [2012]	Y	Y	Y
CLUBB	*Golaz et al.* [2002a,b], *Larson and Golaz* [2005], *Golaz et al.* [2007]	Y	N	N
ECHAM6	*Stevens et al*. [2012]	Y	N	N
ECMWF	*Neggers et al* [2009a; 2009b], *Lock* [2000]	N	Y	Y
EC-ETH	*Brinkop and Roeckner* [1995]	Y	N	N
GFDL-AM3	*Lock* [2000]	N	Y	Y
GISS	*Holtslag and Moeng* [1991]	N	Y	Y
GMAO	*Lock et al.* [2000], *Louis* [1979]	N	Y	Y
HadGEM2	*Lock et al*. [2000]	N	Y	Y
JMA	*Kawai* [2012]	Y	N	N
IPSL	*Loius* [1992], *Houdrin* [2006]	Y	N	Y
RACMO	*Neggers et al* [2009a; 2009b]	N	Y	Y

703

704

705 Table 4: Shallow convection schemes. Some models use the same schemes for deep convections

Models Acronyms	References	Trigger	Lateral entrainment	Lateral detrainment	closure
ACCESS	*Gregory and Rowntree* [1990], *Grant* [2001]	undiluted parcel	specified	specified	TKE
CAM4	*Hack* [1994]	undiluted parcel	N	N	CAPE
CAM5	*Park and Bretherton* [2009]	CIN+TKE	buoyancy sorting	buoyancy sorting	CIN+TKE
CCC	*von Salzen et al.* [2012], *von Salzen and McFarlane* [2002], *Grant* [2001]	undiluted parcel	buoyancy profile	buoyancy profile	CIN+TKE
CLUBB	*Golaz et al.* [2002a;b], *Larson and Golaz* [2005], *Golaz et al.* [2007]	N	N	N	high-order bi-normal distribution
ECHAM6	*Tidietke* [1989]	diluted parcel	specified	specified	Large-scale mass flux
ECMWF	*Tidietke* [1989]	diluted parcel	specified	diagnosed	sub-cloud moist static energy
EC-ETH	*Von Salzen and McFarlane* [2002], *Grant* [2001]	undiluted	buoyancy profile	buoyancy profile	TKE
GFDL-AM3	*Bretherton and Park* [2009]	CIN+TKE	buoyancy sorting	buoyancy sorting	CIN+TKE
GISS	*Del Genio and Yao* [1993]	undiluted parcel	specified	N	CAPE
GMAO	*Moorthi and Suarez* [1992]	undiluted	Diagnosed	N	CAPE
HadGEM2	*Gregory and Rowntree* [1990], *Grant* [2001]	undiluted parcel	specified	specified	TKE
JMA	*Kawai* [2012]	diluted parcel	diagnosed	N	prognostic
IPSL	*Emanuel* [1991]	undiluted parcel	buoyancy sorting	buoyancy sorting	CAPE
RACMO	*Neggers et al* [2009a, 2009b]	unified with PBL scheme	unified with PBL scheme	unified with PBL scheme	unified with PBL scheme

706

707

Figure Captions

Figure 1: Schematics of the experimental setup. The atmospheric temperature and water vapor are constructed based on moist adiabat and fixed relative humidity respectively. The large-scale subsidence is calculated based on the clear-sky thermodynamic equation. These fields change with SST, which is given warming of 2^{o}C in the perturbed climate.

Figure 2: Averaged amount of low clouds in June-July-August (%) from the C3M satellite data. The red line is the northern portion of the GPCI (see text); the symbols "S6", "S11" and "S12" are the three locations studied in the paper.

Figure 3: (a) Large-scale pressure vertical velocity at the three locations in the control climate (solid lines), and in the ERA-Interim (dashed). (b) Same as (a) except that the dashed lines denote subsidence rates in the warmer climate. (c) Same as (b) except for horizontal advective tendency of temperature. (d) Same as (c) except for advective tendency of water vapor.

Figure 4: (a)-(c) are the averaged profiles of cloud amount (%) by SCMs for S6, S11 and S12 respectively (from top to bottom panels). (d)-(f) are the same as (a)-(c) but by the LES models. (g)-(i) are from the C3M satellite measurements. The blue lines are ensemble averages; the red lines are the 25% and 75% percentiles.

Figure 5: Examples of time evolution of cloud amount (%) simulated by JMA (left column) for S6, S11 and S12 respectively from top to bottom panels; CAM4 (middle column); GISS (third column) ; SAMA (right column).

728 Figure 6: Examples of physical tendencies (g/kg/day) of water vapor budget in three SCMs at
729 S11 for the control climate, "*turb*" for turbulence scheme, "*conv*" for convection scheme, "(*c*-*e*)" for
730 net large-scale condensation. The dashed lines are cloud liquid water (0.1g/kg). The black dots show
731 the mid-point of model layers. (a) JMA, (b) CAM4, (c) GISS.

732 Figure 7: (a) Change of cloud radiative forcing (CRF, W/m^2) in SCMs at location S11
733 corresponding to 2^oK SST perturbation. Character "X" above a model's name indicates that the
734 shallow convection scheme is not active; "O" indicates that the shallow convection scheme is active.
735 Models without these characters either do not separately parameterize shallow convection and PBL
736 turbulence, or do not submit results with convection information.

737 Figure 8: (a) Change of moisture tendency in the layer of maximum cloud water (g/kg/day) by
738 the "*Turb*" term from the control climate to the perturbed climate at S11. (b) Same as (a) but for
739 surface latent heat flux (W/m^2).

740 Figure 9: Schematics of cloud feedbacks. Changes of clouds from the control (left) to warmer
741 (right) climates. Blue arrows denote the term of turbulence parameterization in the moisture budget
742 equation; red arrows denote shallow convection; black arrows denote cloud-top entrainment, lateral
743 mixing and dry tiubulence. The sizes of arrows schematically correspond to the magnitude of moisture
744 tendency from the associated processes. (a) Negative cloud feedback, dominated by the increase of
745 surface turbulence. (b) Positive cloud feedback, dominated by the increase of shallow convection or
746 cloud-top entrainment. (c) Cloud feedback from shallow cumulus with sufficient depth, with sign
747 depending on the cloud depth and lateral mixing.

748 Figure 10: Same as Figure 7, but for (a) S6, (b) S12. The models are ordered in the same
749 sequence as in Figure 7. One model (EC_ECH) did not reach quasi-equilibrium state and it is indicated
750 by "N/A".

751 Figure 11: Same as Figure 7 but in LES models. (a) S6; (b) S11; (c) S12.

752

753

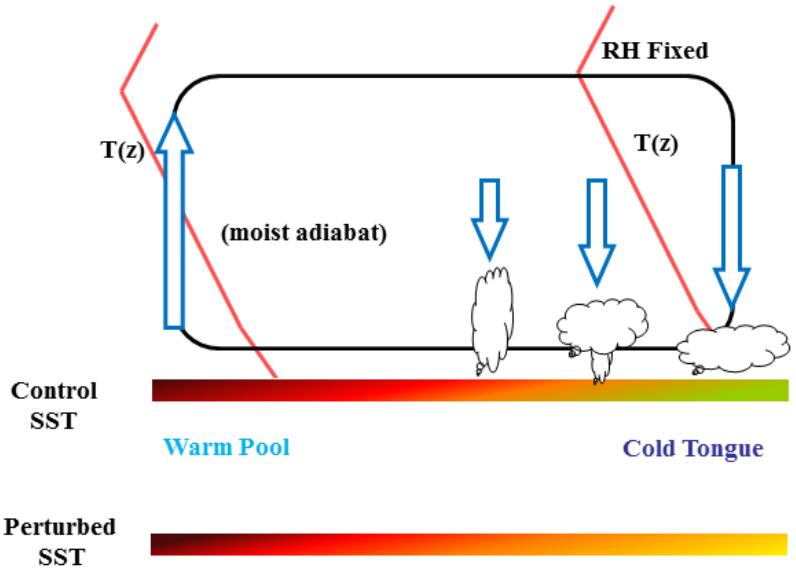

Figure 1: Schematics of the experimental setup. The atmospheric temperature and water vapor are constructed based on moist adiabat and fixed relative humidity respectively. The large-scale subsidence is calculated based on the clear-sky thermodynamic equation. These fields change with SST, which is given warming of 2^{o}C in the perturbed climate.

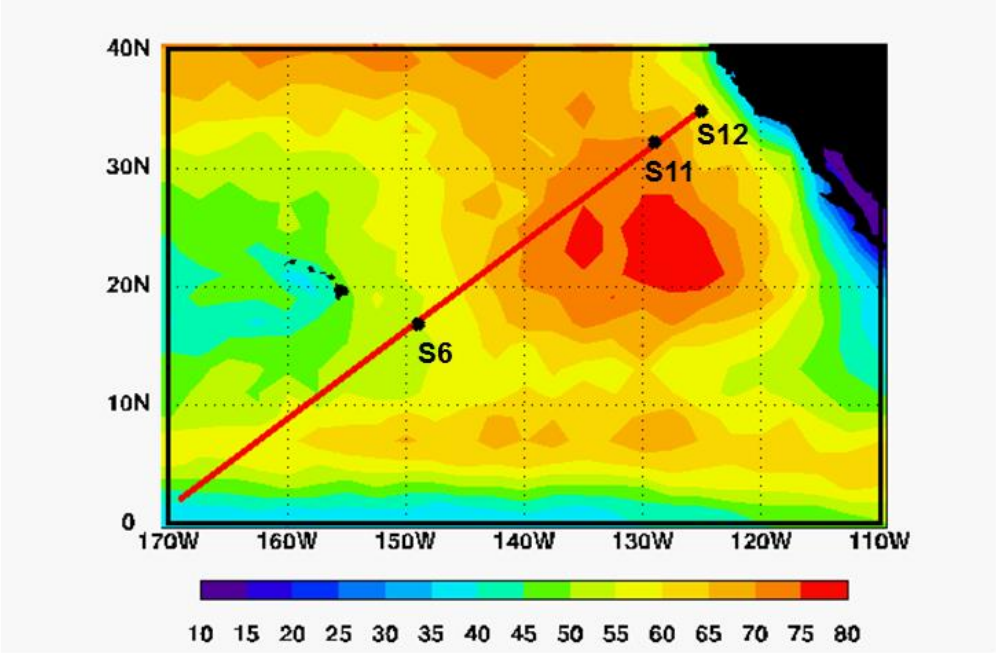

763

764

765 Figure 2: Averaged amount of low clouds in June-July-August (%) from the C3M satellite data. The

766 red line is the northern portion of the GPCI (see text); the symbols “S6”, “S11” and “S12” are the

767 three locations studied in the paper.

768

769

770

771

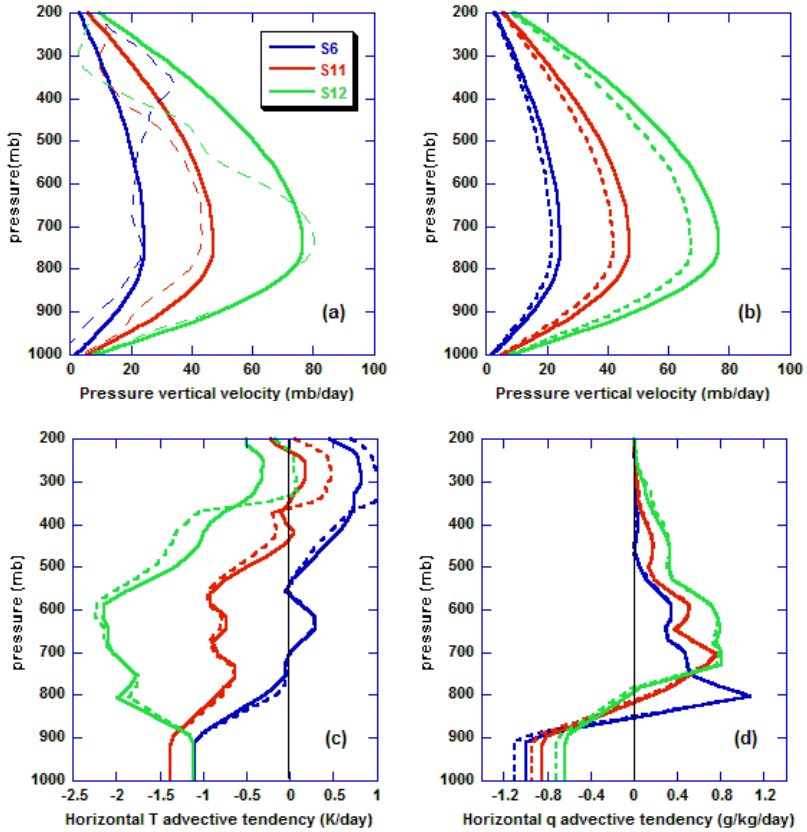

772
773

774 Figure 3: (a) Large-scale pressure vertical velocity (subsidence) at the three locations in the control
775 climate (solid lines), and in the ERA-Interim (dashed lines). (b) Same as (a) except that the dashed
776 lines denote subsidence rates in the warmer climate. (c) Same as (b) except for horizontal advective
777 tendency of temperature. (d) Same as (b) except for horizontal advective tendency of water vapor.

778

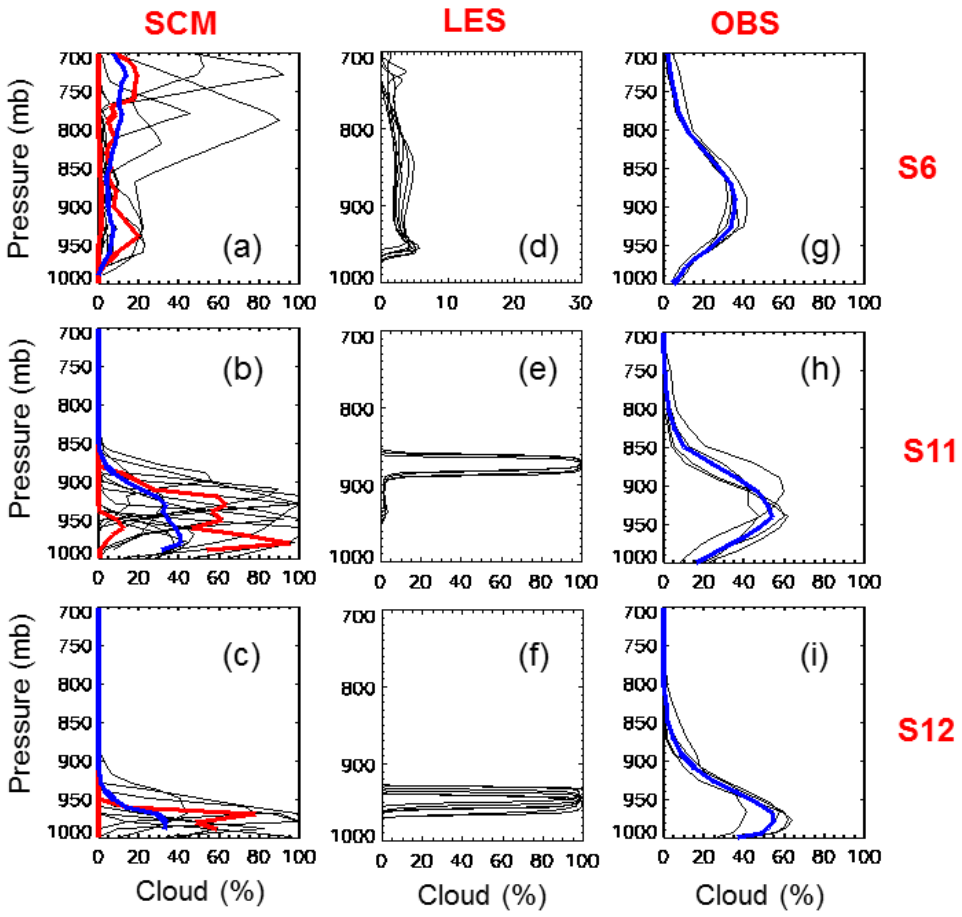

Figure 4: (a)-(c) are the averaged profiles of cloud amount (%) by SCMs for S6, S11 and S12 respectively (from top to bottom panels). (d)-(f) are the same as (a)-(c) but by the LES models. (g)-(i) are from the C3M satellite measurements. The blue lines are ensemble averages; the red lines are the 25% and 75% percentiles.

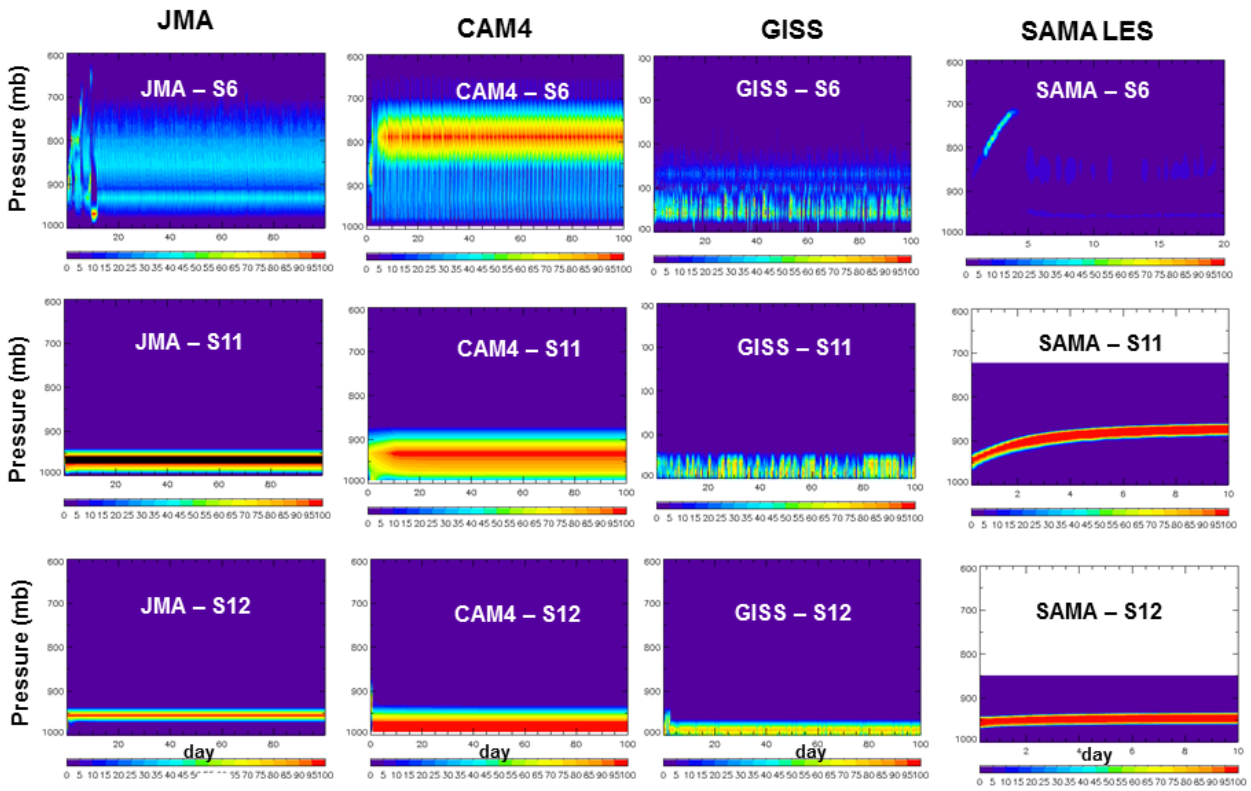

786

787 Figure 5: Examples of time evolution of cloud amount (%) simulated by JMA (left column) for S6,

788 S11 and S12 respectively from top to bottom panels; CAM4 (middle column); GISS (third column);

789 SAMA (right column).

790

791

792

793

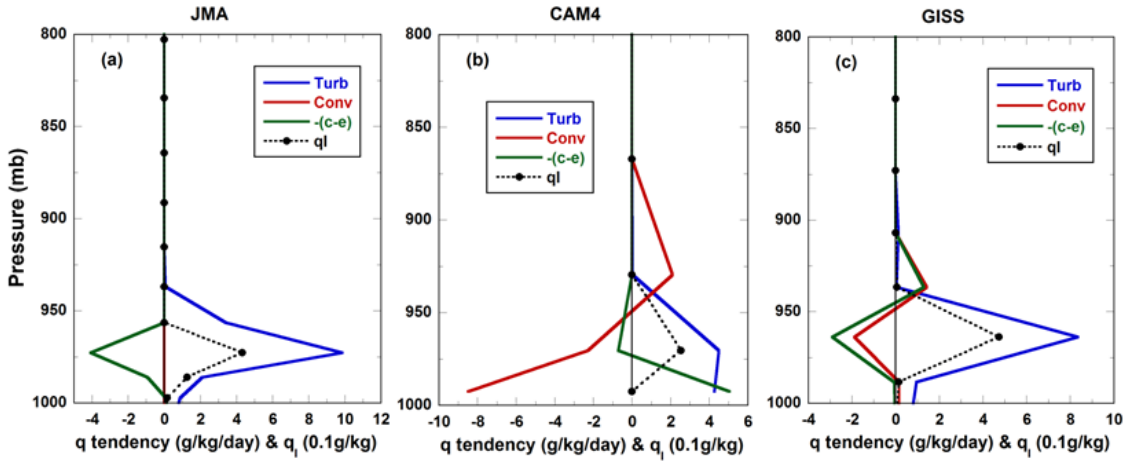

Figure 6: Examples of physical tendencies (g/kg/day) of water vapor budget in three SCMs at S11 for the control climate, "*turb*" for turbulence scheme, "*conv*" for convection scheme, "(*c*-*e*)" for net large-scale condensation. The dashed lines are cloud liquid water (0.1g/kg). The black dots show the mid-point of model layers. (a) JMA, (b) CAM4, (c) GISS.

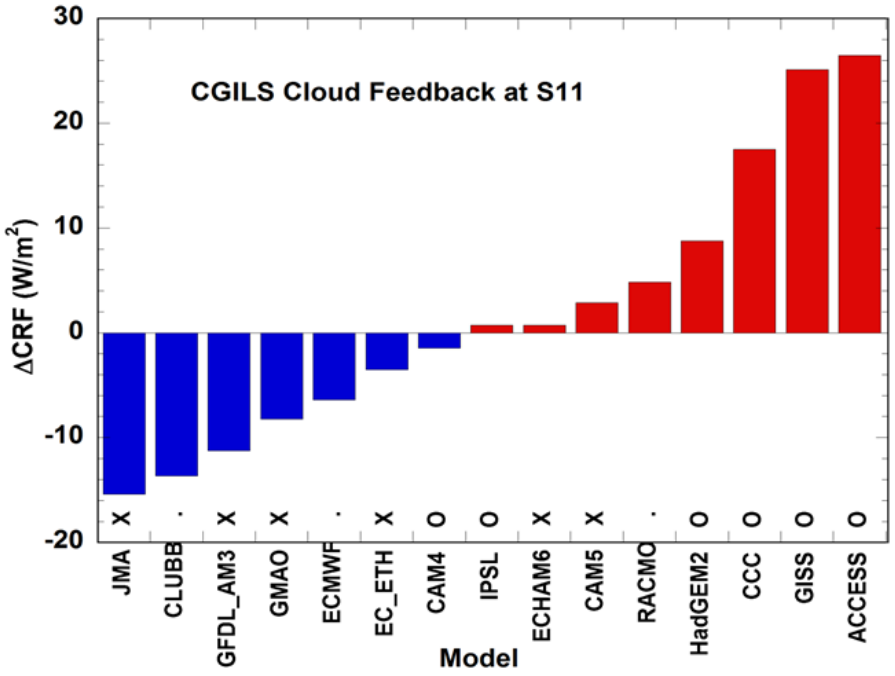

802

803 Figure 7: (a) Change of cloud radiative forcing (CRF, W/m^2) in SCMs at location S11 corresponding
804 to 2^{o}K SST perturbation. Character "X" above a model's name indicates that the shallow convection
805 scheme is not active; "O" indicates that the shallow convection scheme is active. Models without these
806 characters either do not separately parameterize shallow convection and PBL turbulence, or do not
807 submit results with convection information.

808

809

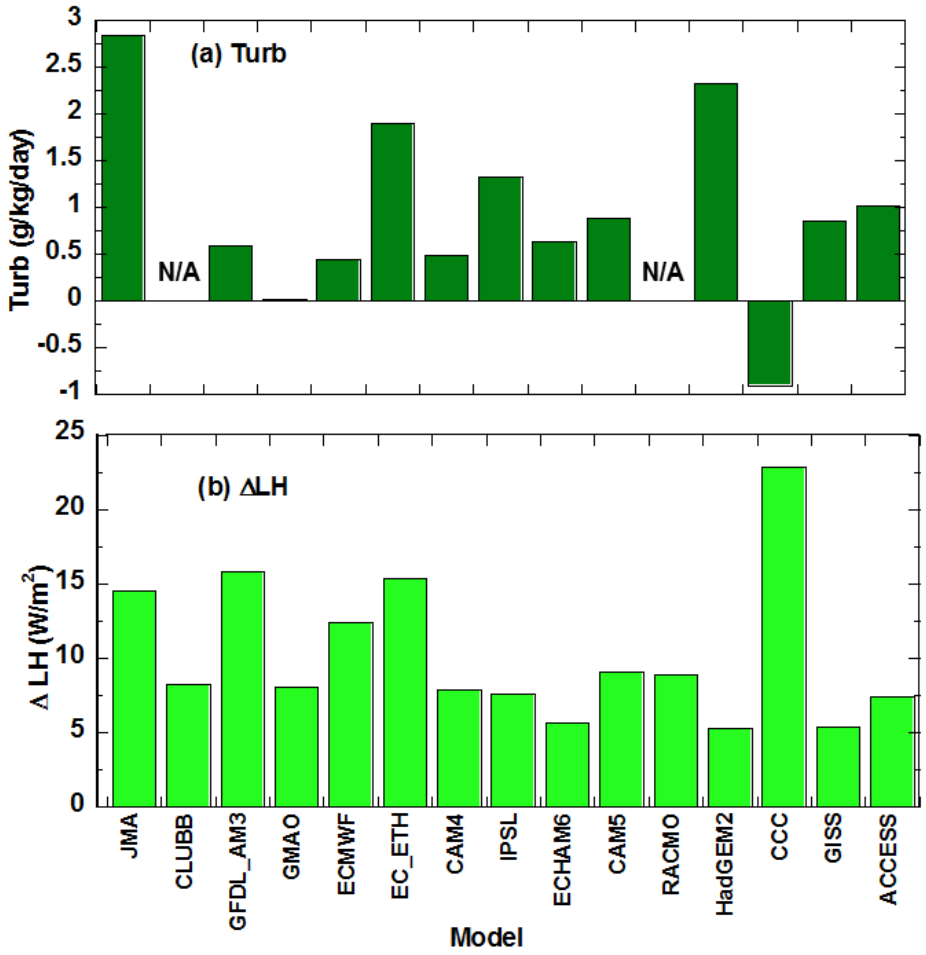

Figure 8: (a) Change of moisture tendency in the layer of maximum cloud water (g/kg/day) by the "*Turb*" term from the control climate to the perturbed climate at S11. (b) Same as (a) but for surface latent heat flux (W/m^2).

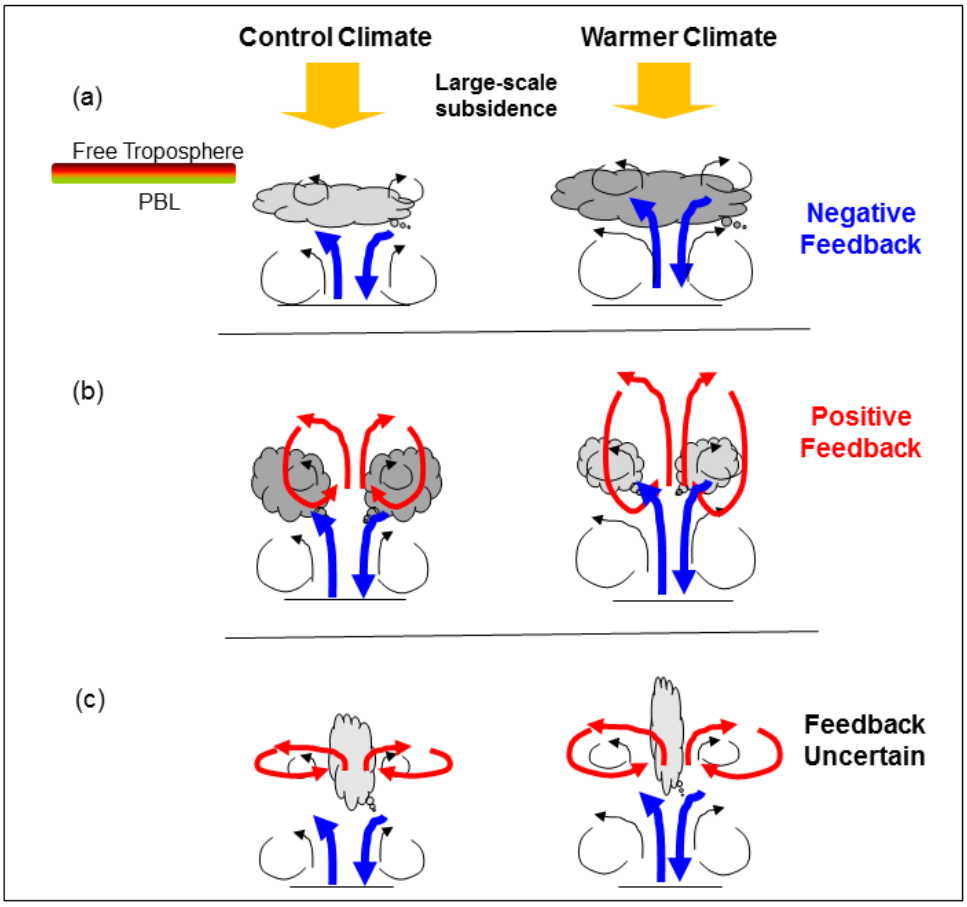

817

818

819 Figure 9: Schematics of cloud feedbacks. Changes of clouds from the control (left) to warmer (right)
820 climates. Blue arrows denote the term of turbulence parameterization in the moisture budget equation;
821 red arrows denote shallow convection; black arrows denote cloud-top entrainment, lateral mixing and
822 dry tiubulence. The sizes of arrows schematically correspond to the magnitude of moisture tendency
823 from the associated processes. (a) Negative cloud feedback, dominated by the increase of surface
824 turbulence. (b) Positive cloud feedback, dominated by the increase of shallow convection or cloud-
825 top entrainment. (c) Cloud feedback from shallow cumulus with sufficient depth, with sign depending
826 on the cloud depth and lateral mixing.

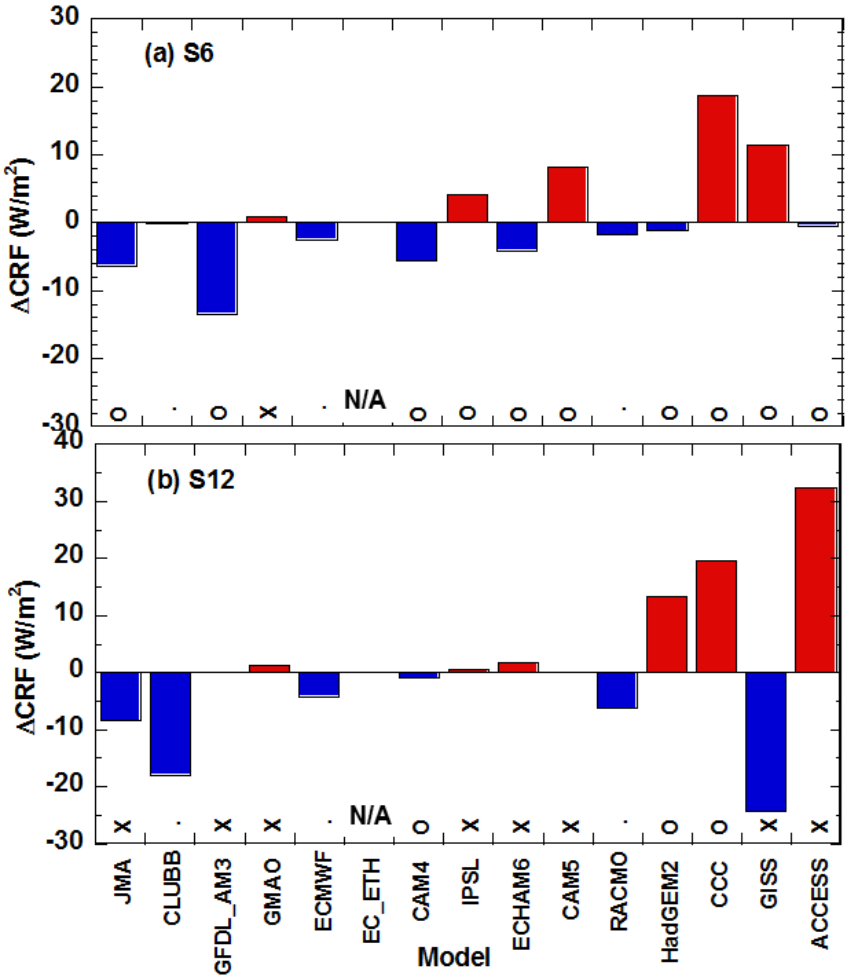

Figure 10: Same as Figure 7, but for (a) S6, (b) S12. The models are ordered in the same sequence as in Figure 7. One model (EC_ECH) did not reach quasi-equilibrium state and it is indicated by "N/A".

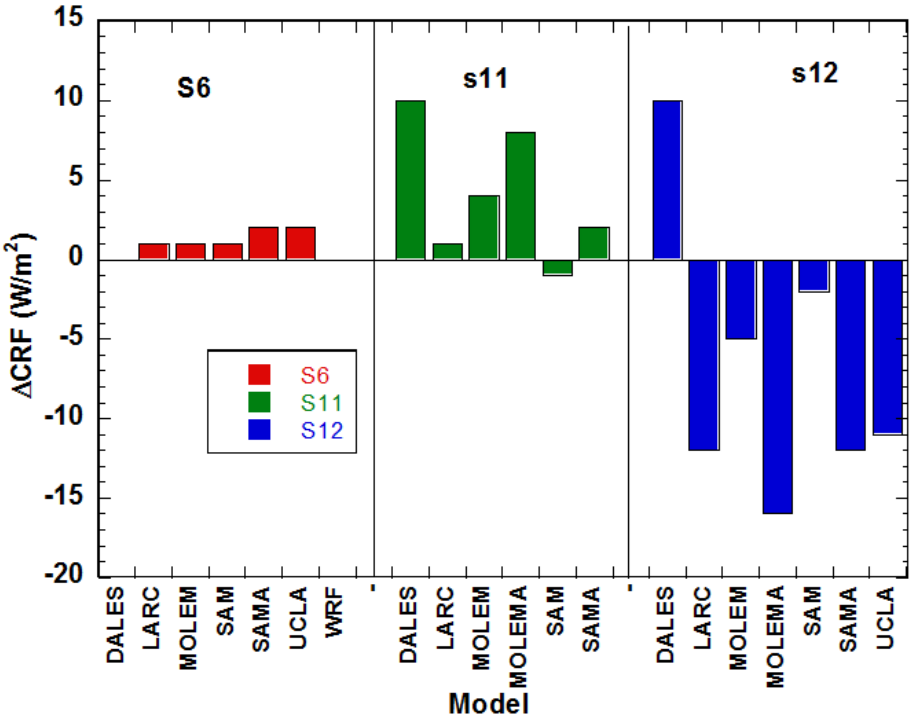

833

834

835 Figure 11: Same as Figure 7 but in LES models. (a) S6; (b) S11; (c) S12.

836